ELSEVIER

Journal of Alloys and Compounds 350 (2003) 136–144

Journal of ALLOYS AND COMPOUNDS

www.elsevier.com/locate/jallcom

Phase changes and hydrogen release during decomposition of sodium alanates

M.P. Balogh[a,*], G.G. Tibbetts[b], F.E. Pinkerton[b], G.P. Meisner[b], C.H. Olk[b]

[a]*General Motors Research and Development Center, Chemical & Environmental Sciences Laboratory, MC 480-106-320, Warren, MI 48090-9055, USA*

[b]*General Motors Research and Development Center, Materials & Processes Laboratory, MC 480-224-320, Warren, MI 48090-9055, USA*

Received 12 June 2002; received in revised form 26 August 2002; accepted 27 August 2002

Abstract

We have constructed a hermetically sealed high-temperature cell for an X-ray diffractometer which allows in situ identification of structural phase changes during the several thermal decomposition stages of sodium alanate materials. Comparing X-ray data with thermogravimetry measurements allows identification of phase changes that correlate with hydrogen release. Measurements made while uniformly ramping up the temperature of purified $NaAlH_4$ indicate that all of the hydrogen release corresponds to the formation of Al or the formation and decomposition of the Na_3AlH_6 phase. The melting of the $NaAlH_4$ phase does not correlate well with sample mass loss in the purified material. For as-received technically pure $NaAlH_4$, hydrogen release lags both Al formation and the formation and decomposition of the Na_3AlH_6 phase. In ball-milled as-received $NaAlH_4$ (ball-milled with diamond powder to achieve ~2 μm crystallite size) there is good correspondence between hydrogen release and either Al formation or the formation and decomposition of the Na_3AlH_6 phase, except that hydrogen release lags the phase changes by a few degrees. For purified $NaAlH_4$ ball-milled in either a steel or tungsten carbide jar, there is a much smaller lag in hydrogen release. For Ti doped material, the phase changes to NaH are completed at the lowest temperature observed in any of the samples, 215 °C, but the TGA measurements are not reliable because of mass loss from decomposition of the catalyst butoxide anion. Among these samples, the delay in hydrogen release does not correlate well with crystallite size; indicating that the delay is not due to hydrogen diffusion, but the delay is definitely decreased by ball milling or adding catalyst material or even impurities.

Keywords: Metal hydrides; Complex hydrides; Hydrogen storage; $NaAlH_4$; Na_3AlH_6

1. Introduction

The automotive industry is now making substantial investments in fuel cell development [1] in the hope that this technology will provide efficient ground transportation as petroleum supplies decrease in the future. In order to avoid the major problems of refining a hydrocarbon fuel in the vehicle, fuel cell vehicles will require a method of storing hydrogen on board. For efficient operation and reasonable range, it has been projected that the storage material should be able to hold at least 6.5 wt% hydrogen [2] and release its sorbed hydrogen below 150 °C.

Our recent studies of carbon nanofibers have convinced us that the best of these materials will store less than 1 wt% hydrogen at room temperature [3,4]. We do not regard this as a promising avenue to explore.

There has been, however, good progress recently in improving the hydrogen storage capacity, sorption kinetics, and temperature behavior of sodium alanates. These materials are inexpensive and can almost meet the DOE 6.5 wt% capacity target [2]. $NaAlH_4$ has been known for many years for its two-step thermal decomposition [5],

$$NaAlH_4 \leftrightarrow 1/3Na_3AlH_6 + 2/3Al + H_2 \quad 3.70\ wt\%\ H_2 \quad (1)$$

$$1/3Na_3AlH_6 + 2/3Al + H_2 \leftrightarrow NaH + Al + 3/2H_2$$
$$1.85\ wt\%\ H_2, \quad (2)$$

providing a total of 5.55 wt% hydrogen at the NaH endpoint. Further decomposition of NaH is not feasible for automotive applications because temperatures over 300 °C are required. Even so, the major drawback in alanate

*Corresponding author.
E-mail address: michael.p.balogh@gm.com (M.P. Balogh).

0925-8388/02/$ – see front matter
PII: S0925-8388(02)00996-9

decomposition according to Eqs. (1) and (2) is that complete decomposition requires temperatures up to 300 °C, while the reverse reaction of Eq. (1) requires very high pressures.

Interest in these materials was reawakened by a 1997 paper by Bogdanović and Schwickardi [6], which showed how reversibility could be catalyzed with transition metals, particularly Ti. Zidan, Takara, Hee and Jensen [7] then reported that doping $NaAlH_4$ with both Ti and Zr lowered the dehydriding temperatures of both stages of decomposition, offering measurable dehydriding below 100 °C. Zaluska, Zaluski, and Ström-Olsen [8] succeeded in accelerating the dehydrogenation kinetics by ball-milling alanates both without additions and with carbon.

Here we seek to understand and compare these improvements by correlating phase changes due to heating measured by X-ray diffraction in purified, as-received, ball-milled, and Ti-doped $NaAlH_4$ materials with the hydrogen release temperatures measured by thermogravimetric analysis.

2. Experiment

2.1. Materials

The as-received $NaAlH_4$ material was purchased from Lancaster Synthesis, Inc. and has a nominal technical purity of 90 wt% with Al and Na_3AlH_6 as the major impurities.

The purified $NaAlH_4$ was synthesized in our laboratory from a 1.0-M solution of commercial $NaAlH_4$ in THF (tetrahydrofuran) prepared using the Shlenk method [9]. Typically, 10 g of $NaAlH_4$ in 100 ml of THF was stirred for 1 h and passed through a glass filter. The filtrate was then concentrated in vacuum to a volume of ~30 ml where $NaAlH_4$ began to crystallize and separate from the solution. One-hundred millilitres of toluene was added to the THF solution and the mixture was stirred for 3 h under an argon atmosphere, causing $NaAlH_4$ to fully separate from the solution as a fine precipitate. The suspension was stirred for another 2 h and filtered. The residue was washed with toluene three times, and then filtered and dried under vacuum overnight at room temperature. After drying, the purified $NaAlH_4$ was obtained as a fine white powder.

The Ti-doped $NaAlH_4$ material was prepared using $Ti[O(CH_2)_3CH_3]_4$. The $NaAlH_4$ was suspended in 200 ml of toluene and stirred at room temperature for 5 h. Then 2 mol% of $Ti[O(CH_2)_3CH_3]_4$ was added and the mixture stirred at 35 °C overnight. Finally, the toluene was evaporated and the residual solid dried overnight under vacuum.

Steel ball-milling was carried out in a Spex 8000 steel mixer mill using two 1.27 cm diameter and four 0.635 cm diameter steel balls of aggregate mass 21 g for a 2-g typical sample size. Steel ball-milling was performed in an O-ring sealed steel jar under 1 atmosphere of Ar. The steel ball-milled as-received $NaAlH_4$ material contained 20 wt% of 6 μm diamond powder and was milled continuously for 1 h. The ball-milled purified $NaAlH_4$ material was fabricated similarly, but to ensure that heating and partial desorption of the hydrogen was minimized, it was milled in 5-min intervals followed by 30 min cooling for a total milling time of ~3 h. The bulk of the purified ball-milled $NaAlH_4$ material remained cooler than 100 °C although impact point temperatures were probably considerably higher. After we discovered substantial Fe in the samples ball-milled in the steel jar, we ball-milled a sample of pure $NaAlH_4$ (no diamond) in a tungsten carbide jar using WC balls and the above 5-min interval techniques for comparison.

2.2. Procedures

Thermogravimetric analysis (TGA) was performed using a Perkin-Elmer System 7 thermogravimetric analyzer. The apparatus was housed in an Ar glove box to protect the air-sensitive samples during loading. Samples ranging from 5 to 14 mg in weight were placed in either a stainless steel or a Pt pan and heated at 1 °C/min from 30 to 300 °C in a 45-sccm flow of Ar.

Real-time in-situ X-ray (XRD) diffraction data were collected using Cu Kα radiation in a Bruker AXS General Area Detector Diffractometer System (GADDS). A special sample cell and furnace, shown in Fig. 1, were designed to minimize oxidation and moisture contamination of these deliquescent materials throughout the diffraction experiment. An XRD capillary tube seals to the brass base with O-rings, and a small passageway connects the capillary tube to the pressure manifold via a quick disconnect fitting.

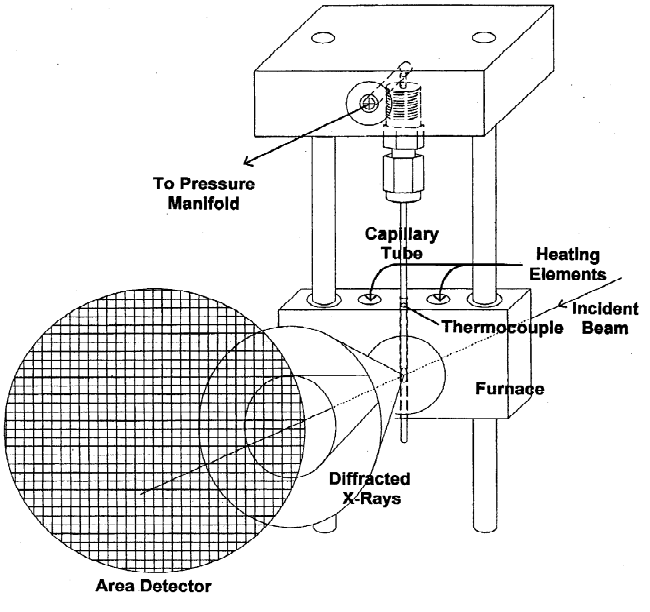

Fig. 1. X-ray diffraction apparatus and scattered X-ray collection geometry used to acquire real-time in situ phase data.

Table 1
X-Ray diffraction parameters used to monitor sample composition

Phase	JCPDF number	Miller indices	Range (2θ)
$NaAlH_4$	73-0088	(112)	28.6–30.2
Na_3AlH_6	20-1072	(020)(112)(200)	31.8–33.2
Al	4-787	(111)	37.4–38.9
NaH	2-809	(111)	30.5–31.8
Diamond	6-675	(111)	43.6–44.6
Background	–	–	24–25

Two posts guide and align the capillary tube in a miniature tube furnace which has two conical windows: one permits the primary X-ray beam access to the sample and the other permits detection of the diffracted and scattered X-ray beams by the GADDS. The sample cell and furnace can be heated to 500 °C, and the temperature is monitored by a thermocouple adjacent to the sample. The temperature at the window of the furnace is about 5% cooler than the furnace block, but the sample temperature could be calibrated using melting point standards to an absolute accuracy of 1%.

Prior to the diffraction measurements, we loaded and sealed the various samples into 1–1.5 mm quartz capillary tubes while inside an inert atmosphere glove box. The XRD data were then collected using a 0.8 mm collimator and a detector distance of 15 cm, with the center of the sample cell at angles $\Omega = 20°$ and $2\theta = 35°$. This allowed collection of integrated diffraction data for angles $17.4° \leq 2\theta \leq 52.3°$. The XRD experiments were performed while heating the various $NaAlH_4$ samples from room temperature to above 400 °C at 2 °C/min in 1 bar of H_2. Diffraction patterns were collected every 30 s, and the observed Debye rings were integrated to give powder diffraction spectra. In some cases, however, the Debye rings were incomplete, consisting of a series of spots due to the relatively large crystallite size compared to the capillary diameter. The compositions of the different samples were monitored from the integrated net intensity of the prominent Bragg reflection for each phase, as listed in Table 1. For Na_3AlH_6, the 2θ apertures are sufficiently large so that phase information on both the α and β phases is collected, but here we make no distinction between the two. Non-crystalline material was monitored by measuring the background intensity. In the case of the ball-milled material, an elevated background was observed and is believed to be a result of fluorescence of iron contaminant introduced during ball-milling.

The materials were also analyzed for metallic contamination after preparation by inductively coupled plasma atomic emission spectroscopy.

3. Results

Fig. 2 shows the relative concentrations of the phases observed as purified $NaAlH_4$ is heated from room temperature to over 300 °C. We observe the clear signature of a melting transition near 180 °C by the disappearance of the diffraction peaks of the $NaAlH_4$. Immediately above this temperature there is a rapid rise in background scattering that we associate with the liquid $NaAlH_4$ phase. Above 210 °C, there is a gradual increase in both the cubic Al reflections and the Na_3AlH_6 reflections. Near 240 °C the Na_3AlH_6 concentration reaches its maximum and simultaneously NaH begins forming. NaH then increases as Na_3AlH_6 decreases, reaching its saturation value near 280 °C.

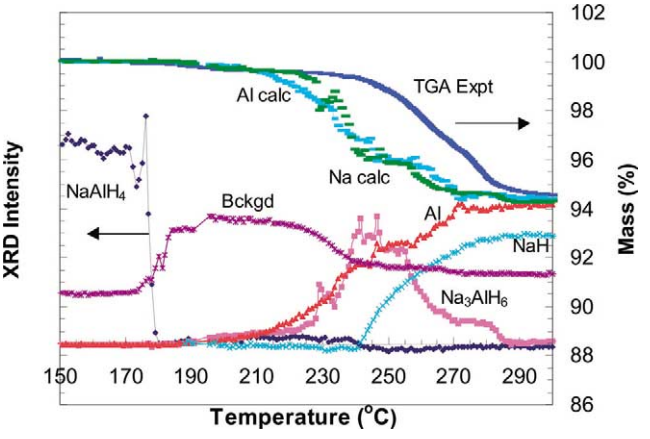

Fig. 2. X-ray diffraction intensities of phases identified during the heating of purified $NaAlH_4$ compared with observed (TGA Expt) and calculated TGA curves based on either the Al (Al calc) or the Na_3AlH_6 (Na calc) intensities.

Superimposed on this plot is the 1 °C/min observed TGA result for mass loss due to H_2 desorption on this plot. Surprisingly, there is no mass loss whatsoever that can be correlated with the disappearance of the $NaAlH_4$ solid phase. The total mass loss seems to correspond with the appearance and disappearance of Na_3AlH_6 and the simultaneous increase in NaH.

As-received $NaAlH_4$ shows qualitatively different behavior on heating (Fig. 3). First, the measurement of $NaAlH_4$ phase concentration shows more noise variation as the temperature is changed because only a small number of the 100-μm grains fit within the X-ray beam. When these shift as temperature is raised, the X-ray diffraction signal fluctuates considerably. The $NaAlH_4$ phase disappears at a slightly lower temperature than for purified $NaAlH_4$. It is replaced not only by an increase in the background scattering, but by an Na_3AlH_6 phase which reaches its maximum concentration near 190 °C, then diminishes gradually and disappears near 255 °C. NaH formation again correlates with Na_3AlH_6 disappearance; NaH concentration becomes appreciable above 210 °C and reaches its maximum near 260 °C. The Al signal also tells a key story; it rises rapidly as the Na_3AlH_6 phase forms near 175 °C and rises again as this phase disappears and NaH forms.

The observed TGA curve for the as-received material is

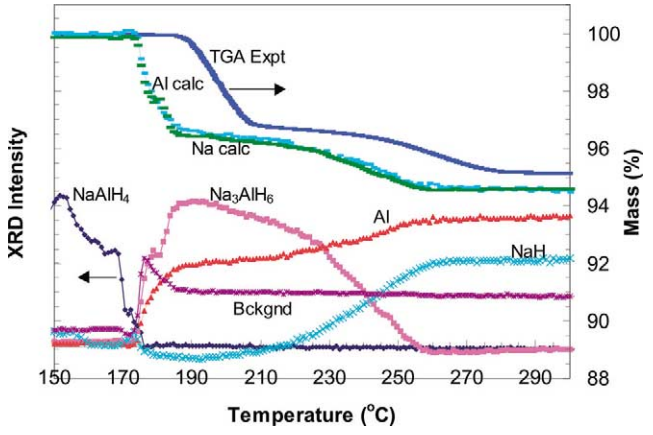

Fig. 3. X-ray diffraction intensities of phases identified during the heating of as-received $NaAlH_4$ compared with observed (TGA Expt) and calculated TGA curves based on either the Al (Al calc) or the Na_3AlH_6 (Na calc) intensities.

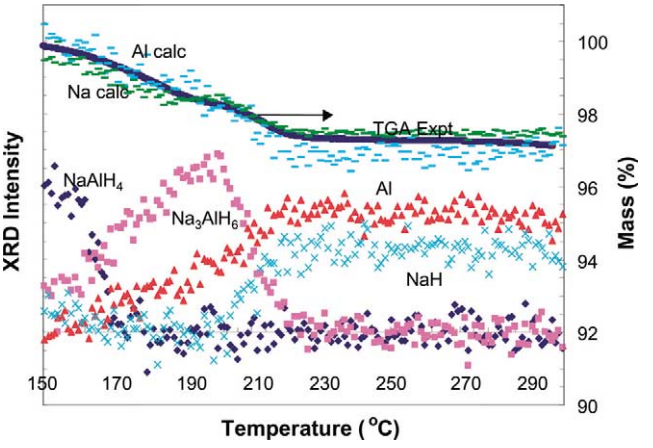

Fig. 5. X-ray diffraction intensities of phases identified during the heating of steel ball-milled purified $NaAlH_4$ compared with observed (TGA Expt) and calculated TGA curves based on either the Al (Al calc) or the Na_3AlH_6 (Na calc) intensities.

consistent with this picture. It shows a somewhat tardy but large mass loss near 190 °C, and a second smaller mass loss between 230 and 270 °C. This TGA result is much more consistent with our expectations based on Eqs. (1) and (2) than was the TGA result for purified $NaAlH_4$.

Data for steel ball-milled as-received $NaAlH_4$ (Fig. 4) are qualitatively similar, but the smaller grain size of about 2 μm gives each phase more overall diffraction intensity and hence a less noisy diffraction signal. The $NaAlH_4$ phase disappears between 160 and 170 °C, while the Na_3AlH_6 phase grows over the same interval, exactly replacing the $NaAlH_4$. In this sample the background

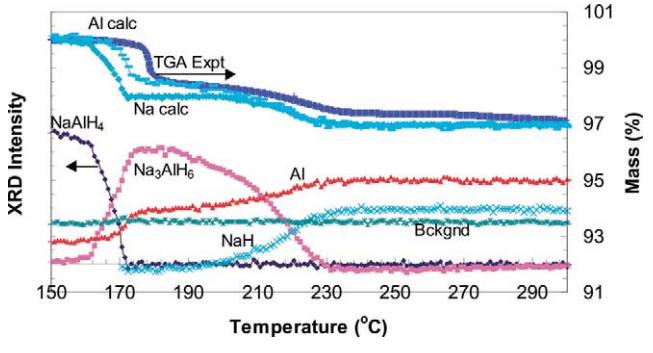

Fig. 4. X-ray diffraction intensities of phases identified during the heating of steel ball-milled as-received $NaAlH_4$ compared with observed (TGA Expt) and calculated TGA curves based on either the Al (Al calc) or the Na_3AlH_6 (Na calc) intensities.

remains constant over the whole temperature range. Furthermore, the Al signal is clearly above zero even before decomposition of the $NaAlH_4$ phase occurs. It then rises sharply at 170 °C where the $NaAlH_4$ phase converts to Na_3AlH_6 and again as the Na_3AlH_6 converts to NaH. The diamond (111) intensity trace is independent of temperature; for simplicity it is not shown on Fig. 4.

Measurements by Inductively Coupled Plasma Atomic Emission Spectroscopy reveal that the steel ball-milled samples gain large amounts of iron during the ball-milling process. As Table 2 shows, the as-received $NaAlH_4$ gains 1.9 wt% Fe during ball-milling. The inert fraction of Ti doped $NaAlH_4$ is listed as 0.113, the mass equivalent of 2 mole% of $Ti[O(CH_2)_3CH_3]_4$, even though we shall see that the butoxide anion decomposes in the temperature range studied here.

The TGA data for steel ball-milled as-received $NaAlH_4$ (Fig. 4) correlate with XRD observations even better than those for as-received $NaAlH_4$, with the low temperature mass loss only a few degrees above the $NaAlH_4$ to Na_3AlH_6 conversion, and a second mass loss correlating well with the formation of NaH. The large X-ray fluorescence associated with the 1.9 wt% of Fe probably accounts for the enhanced X-ray scattered background.

The 3-h slow steel ball-milling of the purified $NaAlH_4$ (Fig. 5) introduces a much larger Fe concentration, 23 wt% (Table 2). The enhanced Fe concentration is accompanied

Table 2
Impurity concentrations in sodium alanate samples

Sample	As-received	Purified	Steel BM as-received	Steel BM purified	WC BM purified	Ti-doped
Diamond (wt%)	0	0	20	20	0	0
Fe (wt%)	0	0	1.9	23	0	0
f (fraction inert)	0	0	0.219	0.43	0	0.113

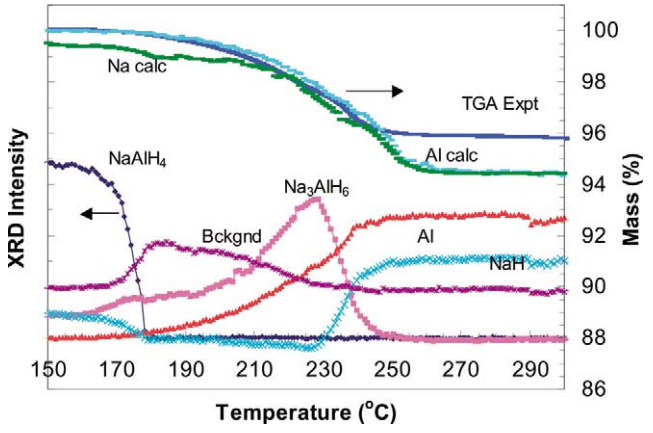

Fig. 6. X-ray diffraction intensities of phases identified during the heating of purified $NaAlH_4$ ball-milled in a WC jar compared with observed (TGA Expt) and calculated TGA curves based on either the Al (Al calc) or the Na_3AlH_6 (Na calc) intensities.

by an increase in the background of scattered X-rays and a loss of X-ray penetration which considerably degrades the signal/noise ratio of the data. Nevertheless, in contrast with the steel ball-milled as-received material, the steel ball-milled purified material does not show perceptible decomposition of the original $NaAlH_4$; neither Al nor Na_3AlH_6 is visible at below 140 °C. However, as Fig. 5 shows, the steel ball-milled purified material decomposes in a mode very similar to that of the steel ball-milled as-received material: $NaAlH_4$ converts to Na_3AlH_6 above 160 °C. Na_3AlH_6 begins growing at 140 °C, but this constituent reaches its maximum near 200 °C, and disappears near 220 °C. Al begins growing as the $NaAlH_4$ disappears at 160 °C, while NaH does not begin to appear until Na_3AlH_6 begins to disappear at 200 °C. All phase changes are complete before 230 °C. The TGA data correspond very nicely with the phase change data.

To determine the behavior of pure $NaAlH_4$ ball-milled with as little impurity as possible, a sample of pure $NaAlH_4$ was ball-milled using a tungsten carbide jar and balls and no diamond addition using the 5-min on (3-h total) procedure. XRD and TGA data for this sample are shown in Fig. 6. The sample shows clear evidence of Na_3AlH_6 at 150 °C, but Na_3AlH_6 does not peak until 228 °C. There is no trace of Al at lowest temperatures, but Al begins growing as $NaAlH_4$ starts to disappear near 170 °C, reaching its maximum near 245 °C. Thus, in the temperature required for Na_3AlH_6, NaH, and Al formation the XRD behavior of this sample is intermediate between the purified material and the steel ball-milled purified sample. Moreover, only in this sample do we observe $NaAlH_4$ pre-decomposition manifested by Na_3AlH_6 formation totally without Al formation. The TGA data resembles that for the purified crystals in that there is no mass loss corresponding to the disappearance of the $NaAlH_4$ phase; the entire mass loss corresponds in temperature to the formation and decomposition of Na_3AlH_6.

Pure $NaAlH_4$ doped with 2 mol% of $Ti[O(CH_2)_3CH_3]_4$ was also studied by these methods. Fig. 7 shows that many of the phase changes occur at the lowest temperatures observed. Solid $NaAlH_4$ disappears completely to form Na_3AlH_6 near 170 °C, and the latter decomposes completely before 220 °C. NaH begins forming at the earliest observed temperature, 175 °C, and reaches its maximum value at 215 °C. However, the TGA results do not clearly track these observations, as mass does not begin dropping until over 180 °C. After an initial drop which is clearly at a

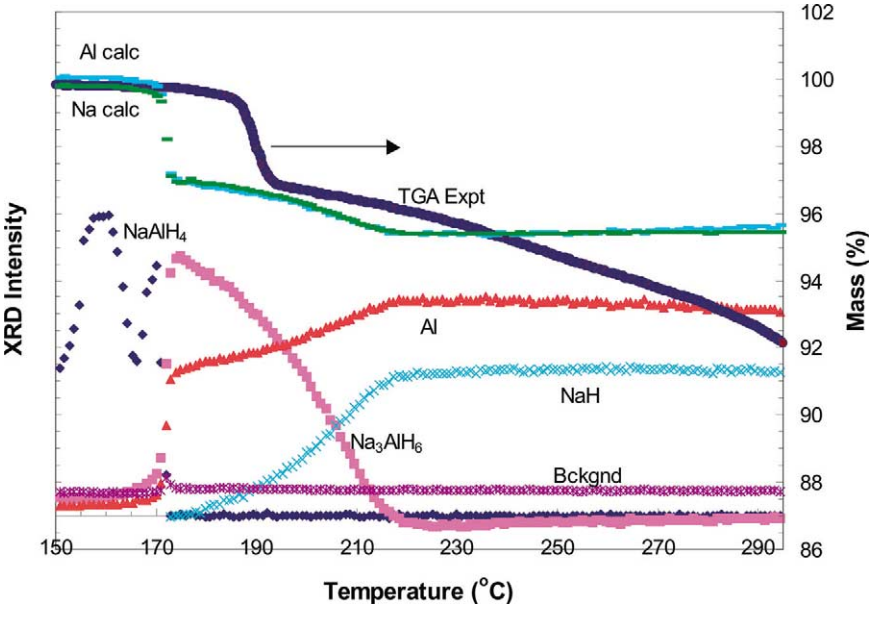

Fig. 7. X-ray diffraction intensities of phases identified during the heating of 2% Ti-doped $NaAlH_4$ compared with observed (TGA Expt) and calculated TGA curves based on either the Al (Al calc) or the Na_3AlH_6 (Na calc) intensities.

temperature above that for conversion of $NaAlH_4$ to Na_3AlH_6, mass is lost at a slow and nearly continuous rate up to 300 °C and beyond. Since this mass loss ultimately extends to more than the 10.6 wt% total H_2 present in the sample, it must correspond to not only the decomposition of the alanates but also the loss of the butoxide anion. This TGA was performed several times with both a Pt pan and a stainless steel pan, with and without a lid, with only minor differences in an effort to detect Na volatilization.

4. Calculated TGA curves

Let us attempt to generate calculated TGA curves from phase changes observed by XRD for quantitative comparison with the observed TGA data. Steel ball-milled as-received $NaAlH_4$ (Fig. 4) shows the most encouraging agreement. The first calculated TGA curve is based on the observed X-ray concentration of Al and the suppositions that:

1. The Al present below 170 °C, Al_0, corresponds to initial decomposition of the $NaAlH_4$ phase after fabrication or during ball-milling.
2. The Al concentration observed above 250 °C, Al_1, corresponds to the complete decomposition of all hydride phases except NaH.
3. Hydrogen (5.55 wt%) is released during the complete formation of Al from the pure alanate. However, a fraction '*f*' of inert material, such as abrasive or catalyst, may be mixed with the sample and lower this number.

The curve in Fig. 4 labeled 'Al calc' is therefore generated by the following formula from the XRD data Al(*T*):

$$Al_{calc}(T) = 100 - 5.55\frac{Al(T) - Al_0}{Al_1}(1-f) \quad (3)$$

A second and partially independent calculated curve may be generated from the formation and disappearance of the Na_3AlH_6 through the suppositions that:

1. Decomposition of the $NaAlH_4$ phase is accompanied by the release of 3.70 wt% hydrogen as Na_3AlH_6 rises from zero to its maximum value $(Na_3AlH_6)_1$.
2. Decomposition of the Na_3AlH_6 phase is accompanied by the release of 1.85 wt% hydrogen as its concentration drops from its maximum to zero.
3. Both of the above phases must be proportionately reduced to account for the fraction Al_0/Al_1 of all hydride decomposed before heating and the inert fraction *f*.

The curve in Fig. 4 labeled 'Na calc' is therefore generated by the following formula from the $Na_3AlH_6(T)$ data:

$$Na_{calc}(T) = 100 - \left[\frac{Al_1 - Al_0}{Al_1}\right] \times \left(3.7\frac{Na_3AlH_6(T)}{(Na_3AlH_6)_1} + 1.85\frac{(Na_3AlH_6)_1 - Na_3AlH_6(T)}{(Na_3AlH_6)_1}\right) \times (1-f) \quad (4)$$

Here the first term in the curved brackets is evaluated only for temperatures below that at which $Na_3AlH_6(T)$ reaches its maximum, while the final term in the curved brackets is evaluated only after $Na_3AlH_6(T)$ reaches its maximum. The curves from Eqs. (3) and (4) show moderately good agreement with each other and with the observed TGA of Fig. 4. The Al calculation underpredicts the first decomposition step by 7 °C, while the Na calculation underpredicts it by 13 °C. Both predict the second decomposition more accurately. By construction they agree on the total decomposition at 300 °C, yet both overestimate only slightly the mass of hydrogen lost at that temperature.

Steel ball-milled purified $NaAlH_4$ (Fig. 5) shows excellent agreement between the two mass loss calculations and the experimental TGA, especially considering the poor signal quality of the XRD data. The calculations do not appear to lag the TGA features.

Fig. 3 shows similar calculations made for as-received $NaAlH_4$. The decomposition is qualitatively similar to steel ball-milled $NaAlH_4$, both as-received (Fig. 4) and purified (Fig. 5), except that the calculations now lag the TGA trace by 20 °C.

In contrast to the above three materials (Figs. 3–5), purified $NaAlH_4$ (Fig. 2) has a distinctly different TGA curve. Even so, the two calculations still give a qualitative approximation to the observed TGA curve, even though they underpredict the desorption temperature by 27 °C or so. For purified $NaAlH_4$, the observed TGA curve agrees with the calculation in that it shows a mass decrease of the full 5.55%. In this case there is neither Al nor inert matter visible in the low temperature XRD data, so there is no correction of the calculated maximum value. The Na calculation is rather noisy because of the large crystallite size of the sample.

For the purified WC ball-milled $NaAlH_4$, (Fig. 6) calculations based on the Na_3AlH_6 signal suffer an immediate 0.5 wt% offset from the experimental TGA signal because the Na_3AlH_6 signal used in Eq. (4) is appreciable at 150 °C. With the exception of this offset and the somewhat noisy Na_3AlH_6 signal, however, agreement between the two calculations and the measured TGA is quite good until 245 °C. However, since the Na_3AlH_6 concentration continues to fall and the Al concentration continues to rise above this temperature, both calculated curves continue to decline while the experimental TGA curve flattens out. Moreover, the two calculated mass loss

curves predict a mass loss of 5.55 wt%, while the observed TGA has a maximum weight loss of 4.2 wt%.

The calculated TGA curves for the Ti-doped $NaAlH_4$ (Fig. 7) are the least satisfactory of the materials tested. Although the TGA curves calculated by both the Na and Al method agree very nicely with each other, neither agrees at all well with the observed TGA curve, lagging the first decomposition by 17 °C. The observed TGA curve does not show any feature which might be associated with the second decomposition; rather, it seems to continuously decrease until well above 300 °C. It seems clear that the observed TGA curve above 230 °C shows some serious sample decomposition which strongly interferes with our ability to calculate the TGA from the XRD phase information. This most likely results from the decomposition of the butoxide catalyst anions.

5. Discussion

Comparison of Figs. 2 and 7 shows a decrease of the temperature at which the alanate completely converts to NaH of 60 °C in the presence of the Ti catalyst. This is in excellent agreement with results observed by Bogdanović and Schwickardi [6] and Jensen, Zidan, Mariels, Hee and Hagen [10]. A similar decrease due to ball-milling of the pure material in Fe crucibles is in agreement with the more qualitative data presented by Zaluska, Zaluski, and Ström-Olsen [8].

A recent paper by Gross, Guthrie, Takara, and Thomas [11] utilized somewhat different equipment to obtain X-ray diffraction phase identification data on purified and catalyzed $NaAlH_4$. Our results differ with theirs in some details. Gross et al. [11] observed rapid and reversible changes in the $NaAlH_4$ peak intensities upon warming, and attributed them to distortions in the crystal lattice. Examination of our figures shows very large $NaAlH_4$ peak intensity fluctuations in Fig. 3, lower fluctuations in Fig. 2, and least in Fig. 4; the fluctuations decrease as crystallite size decreases from 100 to 20 to 2 μm. We believe these fluctuations are large when a small number of large crystallites expand with heating and shift in and out of the diffracting condition. With the ball-milled 2 μm material, positional movements average out, and only small fluctuations are seen.

Furthermore, we do not see any trace of either the X_1 or X_2 phase observed by Gross et al. [11]. We do, however, see traces of $NaSiO_3$ and a complex Na–Al silicate forming over 400 °C which we believe incorporate silicates from the sample tube. Perhaps the suggestion of Gross et al. that the X_2 phase may incorporate Be from their window is correct.

Let us take a somewhat deeper look at what the TGA modeling calculation reveals about decomposition in sodium alanates. For all samples except the Ti catalyzed:

In general the normalization of our TGA calculations ranges from good to acceptable. For purified $NaAlH_4$, because the observed TGA curve shows hydrogen release very close to the stoichiometric 5.55 wt%, the model by construction fits the high-temperature endpoint closely. For both iron ball-milled materials, the TGA experiment is overestimated only slightly by the two calculations. For as-received $NaAlH_4$, the model overestimates the high-temperature TGA weight loss by about 10%, which corresponds to the nominal purity of the material. For WC ball-milled pure material the TGA decomposition is somewhat less than that obtained from the two calculations. This sample is anomalous in that the absence of any low temperature Al signal indicates that ball-milling did not decompose a measurable amount of $NaAlH_4$, while the appreciable low temperature Na_3AlH_6 signal indicates that about 16% of the sample has already converted to Na_3AlH_6. This explains why the Na calc curve starts at somewhat below 100%.

Because the XRD data detects only Al crystallites of appreciable lattice coherence length, and cannot in principle measure dissolved Al or very small aggregates of Al atoms, the number Al_0 which we determine from the low temperature Al X-ray signal is an underestimate of all initial free Al. Therefore, Eqs. (3) and (4) should, as they do, overestimate the total decomposition which the TGA experiment measures. This overestimate is most extreme in the as-received and WC ball-milled pure $NaAlH_4$, indicating that many Al atoms present in this sample are dispersed too broadly to scatter X-rays and appear as XRD data. These Al atoms presumably come from very slow decomposition of the $NaAlH_4$ at room temperature, and cannot easily aggregate at low temperatures. This is also the likely explanation for the absence of Al observed at 150 °C in the WC ball-milled purified $NaAlH_4$ where the Na_3AlH_6 shows a signal appreciable above 0. Proper normalization of the calculated TGA traces would move them closer to the experimental curve.

Thus, the decomposition of as-received $NaAlH_4$ and all three ball-milled $NaAlH_4$ materials seems to be consistent with Eqs. (1) and (2) above, with hydrogen release correlating to a certain extent with the formation and decomposition of Na_3AlH_6. The formation of Na_3AlH_6 can occur at various temperatures for materials prepared by different methods, but it is always in better agreement with the formation of Al crystallites. This seems to be in agreement with the suggestion of Gross et al. [11] that hydrogen is primarily bonded as AlH_3. They suggested recasting Eqs. (1) and (2) as

$$(NaH)(AlH_3) \leftrightarrow 1/3\,(NaH)_3(AlH_3) + 2/3\,(AlH_3) \leftrightarrow (NaH) + (AlH_3) \quad (6)$$

$$AlH_3 \leftrightarrow Al + 3/2H_2, \quad (7)$$

which clearly have the desired form. In the purified $NaAlH_4$ the AlH_3 seems to be much more long lived than

in the other two samples, perhaps because of the absence of catalysts or surface active sites, and therefore requires much higher temperatures for its decomposition and the release of hydrogen.

Adding to these complications is the fact that the delayed release of hydrogen during the thermal decomposition of alkali metal alanates is strongly affected by the slow kinetics of decomposition. Our experiments with $LiAlH_4$ show that increasing the heating rate by a factor of 10, from 0.2 to 2 °C/min increases the observed decomposition temperatures by about 28 °C. For a simple two-fold increase in the ramp rate, a lag of about 9 °C is evident. Nevertheless, the TGA temperatures are still retarded compared to the phase change temperatures by about 10 °C. Under these conditions our choice of 1 °C/min as a ramp rate for the TGA experiments and 2 °C/min for the ramp rate of the XRD phase change experiments may seem rather awkward. However, it should be noted that this selection should make the phase change data lag the TGA data, which is the opposite of our observations in every experiment. Moreover, the observation that our mass loss lags vary widely from sample to sample underscores the fact that the temperature lag is very specifically materials dependent.

One might hope that the delayed release of hydrogen observed in the TGA experiments compared to temperatures at which phase changes occur might be understandable based on the mobility of hydrogen in the alanate lattice. Qualitatively consistent with this idea is the observation that the most finely ground purified ball-milled material exhibits prompt hydrogen release while the as-received ball-milled material exhibiting 10 °C delay has 2 μm crystallite size. As-received $NaAlH_4$ with a 20 °C delayed release has 100 μm crystallite size, as observed by scanning electron microscopy [12]. However, purified $NaAlH_4$, which exhibits the largest (27 °C) delayed release, has an intermediate crystallite size of 20 μm. Moreover, calculations based on hydrogen diffusion rates out of a spherical sample [13], approximating the diffusion coefficients with those for H in Pd or Ni [14], give hydrogen equilibration times of less than 10 s even for the 100-μm crystallites. Slow hydrogen mobility through the crystallite, thus, does not appear to account for tardy hydrogen release. It seems likely that iron ball-milling accelerates hydrogen release partially through Fe catalysis. This is also consistent with the somewhat lower decomposition temperatures observed for every phase of the iron ball-milled purified material with 23 wt% Fe than for ball-milled as-received $NaAlH_4$ with 1.9 wt% Fe.

Ti-doping appears to be similar to Fe doping in that the decomposition of the $NaAlH_4$ phase appears nearly complete at 170 °C; it is superior to Fe doping in that NaH phase is completely formed at 215 °C rather than 230 °C.

We will present two plots in an effort to generalize the effect of the various sample preparation procedures discussed here. The first compares the temperature at which Na_3AlH_6 reaches its maximum for the different samples. This maximum may be precisely defined from the data and, as we have seen, approximates the mid-point in hydrogen desorption temperature. The top panel of Fig. 8 shows that Na_3AlH_6 in the as-crystallized purified material maximizes at by far the highest temperature, and that ball-milling alone in the WC jar lowers the temperature about half as much as ball-milling in a steel crucible with its consequent Fe addition. Na_3AlH_6 in the as-received material in its original crystallized form reaches a maximum at a much lower temperature, which, nevertheless, is lowered still more by ball-milling in a steel jar. Na_3AlH_6 in the Ti doped purified material maximizes at the lowest temperature, barely above the melting temperature of as-received $NaAlH_4$.

A second plot (Fig. 8, bottom) shows the temperature difference by which the average of the two calculated curves lead the TGA experimental curve at the midpoint of the first discernible desorption. This ‘retardation’ measures how much later in temperature the hydrogen leaves the sample after XRD determines a phase change. This retardation temperature is greatest for the samples composed of large crystallites, although it does not exactly correspond to crystallite size. It is substantially smaller for both types of ball-milled samples.

In conclusion, the purified material is quite difficult to decompose: WC ball-milling can drop the decomposition temperature somewhat, but steel ball-milling lowers the

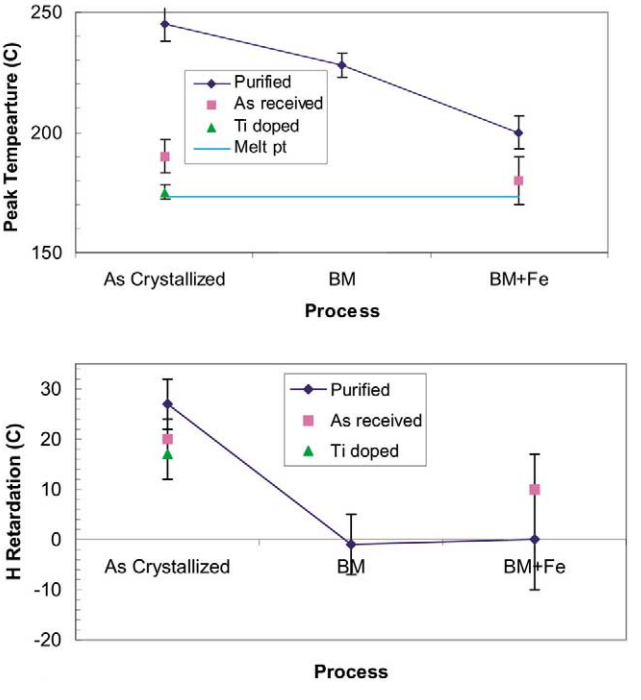

Fig. 8. (Top) Temperature during a 2 °C/min temperature sweep in 1 atm of hydrogen at which the Na_3AlH_6 XRD line reaches its maximum, plotted as a function of processing parameters. (Bottom) Temperature by which the TGA measurement of hydrogen release lags the model values calculated from the XRD data.

decomposition temperature even further. Ti doping is about the best procedure of all. Surprisingly, the as-received 90% pure material decomposes at nearly as low a temperature as the Ti catalyzed material, particularly after iron ball-milling.

Acknowledgements

Many thanks to Dr. Bouziane Yebka for providing the purified and Ti catalyzed $NaAlH_4$ materials and for useful discussions. Thanks also to Noel Potter for the inductively coupled plasma atomic emission spectroscopy measurements and to Kathleen Taylor and Jan Herbst for many helpful suggestions.

References

[1] P. Fairley, Technol. Rev., November/December (2000) 54.
[2] S. Hynek, W. Fuller, J. Bentley, Int. J. Hydrogen Energy 22 (1997) 601.
[3] G.G. Tibbetts, G.P. Meisner, C.H. Olk, Carbon 39 (2001) 2291.
[4] F.E. Pinkerton, M.S. Meyer, G.G. Tibbetts, Proceedings of the 11th Canadian Hydrogen Conference, Victoria, BC, 2001.
[5] C.M. Jensen, K.J. Gross, Appl. Phys. A 72 (2001) 213.
[6] B. Bogdonavić, M. Schwickardi, J. Alloys Comp. 253 (1997) 1.
[7] R.A. Zidan, S. Takara, A.G. Hee, C.M. Jensen, J. Alloys Comp. 285 (1999) 119.
[8] A. Zaluska, L. Zaluski, J.O. Ström-Olsen, J. Alloys Comp. 298 (2000) 125.
[9] D.F. Shriver, The Manipulation of Air-Sensitive Compounds, John Wiley & Sons, New York, 1986.
[10] C.M. Jensen, R. Zidan, N. Mariels, A. Hee, C. Hagen, Int. J. Hydrogen Energy 24 (1999) 461.
[11] K.J. Gross, S. Guthrie, S. Takara, G. Thomas, J. Alloys Comp. 297 (2000) 270.
[12] G.P. Meisner, G.G. Tibbetts, C.H. Olk, M.P. Balogh, Enhancing Low Pressure Storage in Sodium Alanates, J. Alloys Comp. 337 (2002) 254.
[13] J. Crank, The Mathematics of Diffusion, in: Oxford U. Press, London, 1975, p. 91.
[14] W. Jost, Diffusion in Solids, Liquids, and Gases, in: Academic Press, New York, 1952, p. 175.